

Entropic Mirror Monte Carlo

Anas Cherradi^{1,2}, Yazid Janati El Idrissi³, Alain Durmus⁴, Sylvain Le Corff¹,
Yohan Petetin⁵, and Julien Stoehr^{6, 7}

¹Sorbonne Université, Université Paris Cité, CNRS, Laboratoire de Probabilités, Statistique et Modélisation, LPSM, 75005 Paris, France

²EMINES, University Mohammed VI Polytechnic, Benguerir, Maroc

³Institute of Foundation Models, MBZUAI, 75002 Paris, France

⁴Centre Mathématiques Appliquées, Institut Polytechnique de Paris, 91120 Palaiseau, France

⁵Telecom SudParis, CNRS, Institut Polytechnique de Paris, 91011 Evry, France

⁶CEREMADE, Université Paris-Dauphine, Université PSL, CNRS, 75016 Paris, France

⁷Université Paris-Saclay, INRAE, AgroParisTech, UMR MIA Paris-Saclay, 91120 Palaiseau, France

Abstract

Importance sampling is a Monte Carlo method which designs estimators of expectations under a target distribution using weighted samples from a proposal distribution. When the target distribution is complex, such as multimodal distributions in high-dimensional spaces, the efficiency of importance sampling critically depends on the choice of the proposal distribution. In this paper, we propose a novel adaptive scheme for the construction of efficient proposal distributions. Our algorithm promotes efficient exploration of the target distribution by combining global sampling mechanisms with a delayed weighting procedure. The proposed weighting mechanism plays a key role by enabling rapid resampling in regions where the proposal distribution is poorly adapted to the target. Our sampling algorithm is shown to be geometrically convergent under mild assumptions and is illustrated through various numerical experiments.

Keywords. adaptive importance sampling, mirror descent

1 Introduction

Let π be a probability distribution on $\mathcal{X} = \mathbb{R}^d$, known up to a multiplicative constant. Our objective is to estimate expectations of the form $\pi(f) = \int f(x)\pi(dx)$ for measurable test functions f , in settings where direct sampling from π is infeasible. Such situations naturally arise in Bayesian inference, rare event simulation and high-dimensional statistical modelling.

A standard methodology for addressing this problem is importance sampling. Given a proposal distribution μ that dominates π , expectations under π can be approximated by reweighting samples drawn from μ . The statistical efficiency of importance sampling critically depends on the mismatch between μ and π . In particular, it is well known that the mean squared error of self-normalized importance sampling estimators can grow exponentially with divergence measures such as the Kullback–Leibler or Rényi divergences between π and μ [Agapiou et al., 2017, Chatterjee and Diaconis, 2018]. This phenomenon severely limits the applicability of importance sampling in high-dimensional settings or when π exhibits strong multimodality. In Grenioux et al. [2025], the authors highlight in particular that addressing multi-modality is a major challenge of sampling algorithms and discuss systematic evaluation of various samplers.

Adaptive importance sampling methods aim to mitigate this issue by iteratively updating the proposal distribution using weighted samples from previous iterations [Oh and Berger, 1993, Cappé et al., 2004, Cornuet et al., 2012]. These approaches typically rely on parametric or non-parametric families of distributions and on variational criteria such as the minimization of the Kullback–Leibler divergence. Despite significant progress, designing adaptive proposals that simultaneously scale with the dimension and efficiently explore multimodal target distributions remains a challenging problem.

Markov chain Monte Carlo methods provide an alternative strategy by constructing a Markov chain that admits π as invariant distribution. These methods avoid the need to evaluate the normalizing constant of π and enjoy strong asymptotic guarantees [Roberts and Rosenthal, 2004]. However, in practice, their performance is often hindered by poor mixing properties, especially in multimodal settings where transitions between distant regions of high probability mass are unlikely. Moreover, while Markov chain Monte Carlo algorithms generate asymptotically exact samples, they do not directly yield tractable proposal distributions that can be evaluated pointwise, which prevents their direct use within importance sampling frameworks.

A promising direction to overcome these limitations consists in constructing sequences of probability measures $\{\mu_t\}_{t \in \mathbb{N}}$ that progressively approach the target distribution while enjoying explicit contraction properties. Recent works have shown that Entropic Mirror Descent mappings provide a principled way to define such sequences, ensuring a geometric decrease of $\text{KL}(\pi \parallel \mu_t)$ under suitable conditions [Beck and Teboulle, 2003, Dai et al., 2016, Korba and Portier, 2022]. However, the resulting updates are typically intractable and difficult to approximate in multimodal settings, as naive Monte Carlo approximations may fail to discover regions of high probability mass.

In this paper, we propose a new adaptive importance sampling methodology, coined *Entropic Mirror Monte Carlo* (EM2C). Our approach augments the Entropic Mirror Descent transformation with Markovian dynamics that promote exploration while preserving contraction properties. The resulting mapping combines weighted samples drawn from the current proposal distribution with samples propagated through a Markov transition kernel. This construction yields a sequence of idealized updates that converges geometrically fast to the target distribution under mild assumptions. We further derive a practical stochastic implementation based on sampling, weighting and resampling steps, and demonstrate through numerical experiments that the proposed method efficiently handles challenging multimodal targets, including in high-dimensional settings.

The main contributions of this work can be summarized as follows.

- We propose a sequence of idealized updates for the proposal distributions that converges geometrically fast to the target distribution under mild assumptions. Each update is formulated as a mixture of two components: the first preserves the contraction properties of Entropic Mirror Descent and exploits regions already well represented by the current proposal, while the second leverages the exploratory capabilities of a Markov kernel.
- We show that, although the Unadjusted Langevin kernel induces a bias with respect to its invariant distribution, this bias remains controlled and does not hinder convergence, while the contraction effect of the entropic mirror descent component is preserved.
- We introduce a novel importance sampling scheme to approximate the idealized algorithm and demonstrate its effectiveness through numerical experiments in various settings.

The paper is organized as follows. In Section 2, we present how to construct a sequence of probability measures that converges to the target distribution and enjoys explicit contraction guarantee and detail Entropic Mirror descent. In Section 3, we introduce our stochastic imple-

mentation of Entropic Mirror Monte Carlo in Algorithm 1. The empirical performance of the algorithm are provided in Section 4.

2 Entropic Mirror descent

Notations and conventions. Throughout the paper, the state space is $\mathcal{X} = \mathbb{R}^d$ and the reference dominating measure is the Lebesgue measure Leb . We denote by $\mathbb{M}_1(\mathbb{R}^d)$ the set of probability measures on \mathbb{R}^d and by

$$\mathbb{M}_\pi = \left\{ \mu \in \mathbb{M}_1(\mathbb{R}^d) : \pi \gg \mu \text{ and } \mu \gg \pi \right\}$$

the set of probability measures that are equivalent to π .

We do not distinguish probability measures from their densities with respect to Leb . Accordingly, when $\mu \ll \text{Leb}$, we write $\mu(dx) = \mu(x) \text{Leb}(dx)$. For $\nu \in \mathbb{M}_\pi$, the Radon–Nikodym derivative of π with respect to ν is given, for for ν -almost every x , by

$$\frac{d\pi}{d\nu}(x) = \frac{\pi(x)}{\nu(x)}.$$

For any probability measure ν and measurable function f , we use the shorthand

$$\nu(f) = \int_{\mathcal{X}} f(x) \nu(dx), \quad \|f\|_\infty = \sup_{x \in \mathbb{R}^d} |f(x)|.$$

Given a Markov transition kernel K on $(\mathbb{R}^d, \mathcal{B}(\mathbb{R}^d))$ and a probability measure μ , we define

$$\mu K(dy) = \int \mu(dx) K(x, dy).$$

A Markov kernel K is said to be π -invariant if $\pi K = \pi$.

The Kullback–Leibler between π and $\mu \in \mathbb{M}_\pi$ is defined as

$$\text{KL}(\pi \parallel \mu) = \int \log \frac{d\pi}{d\mu}(x) \pi(dx).$$

Finally, the total variation distance between two probability measures μ and ν is defined as

$$\|\mu - \nu\|_{\text{TV}} = \sup_{A \in \mathcal{B}(\mathbb{R}^d)} |\mu(A) - \nu(A)|.$$

2.1 Contracting sequences of probability measures

Our objective is to construct a sequence of probability measures $\{\mu_t\}_{t \in \mathbb{N}}$ in \mathbb{M}_π that converges to the target distribution π and enjoys explicit contraction guarantees. More precisely, we seek sequences satisfying, for some constant $0 \leq \rho \leq 1$ and all $t \in \mathbb{N}$,

$$\text{KL}(\pi \parallel \mu_{t+1}) \leq \rho \text{KL}(\pi \parallel \mu_t). \tag{1}$$

When $\rho < 1$, this property ensures that $\text{KL}(\pi \parallel \mu_t)$ converges geometrically fast to zero.

We focus on sequences generated as iterates of a mapping $\mathcal{F} : \mathbb{M}_\pi \rightarrow \mathbb{M}_\pi$,

$$\mu_{t+1} = \mathcal{F}(\mu_t),$$

and refer to such a mapping as *contracting* when (1) holds. Recent works have shown that mirror descent–type mappings provide a principled way to construct such sequences [Beck and Teboulle, 2003, Dai et al., 2016, Daudel et al., 2021, Korba and Portier, 2022].

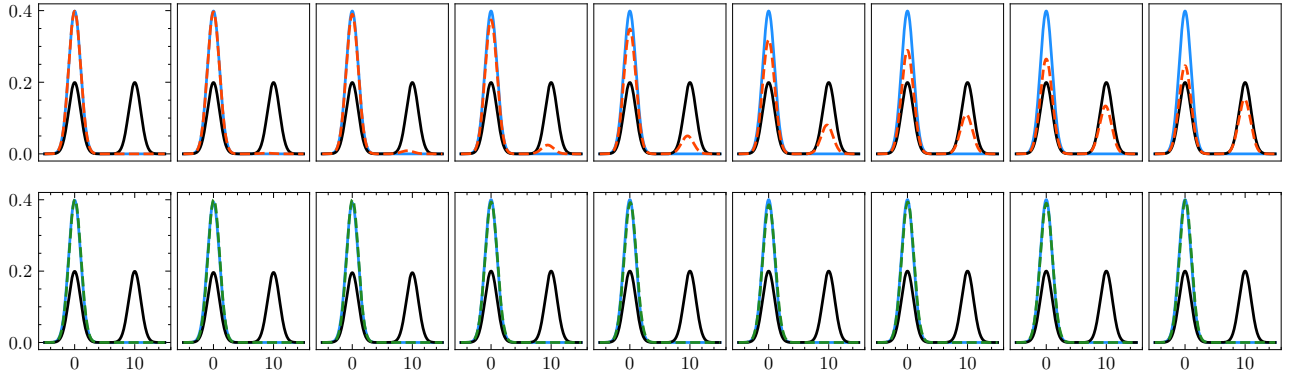


Figure 1: Intermediate sequence of proposal distributions build with the Entropic Mirror Descent for sampling from the bimodal target distribution $\pi = 0.5 \cdot \mathcal{N}(0, 1) + 0.5 \cdot \mathcal{N}(10, 1)$ (black solid line) and starting with distribution μ_0 (blue solid line). Top row: theoretical sequence $\{\mu_t\}_{t \geq 0}$ (red dashed line). Bottom row: updates (green dashed line) when using a bimodal variational distributions build upon 5000 samples from $\{\mu_t\}_{t \geq 0}$.

2.2 Entropic Mirror Descent mapping

For all $\mu \in \mathbb{M}_\pi$ and $0 < \varepsilon \leq 1$, the Entropic Mirror Descent mapping \mathcal{F}_e is defined as

$$\mathcal{F}_e(\mu) \propto \left(\frac{d\pi}{d\mu} \right)^\varepsilon \mu. \quad (2)$$

The mapping \mathcal{F}_e corresponds to a particular instance of mirror descent applied to the minimization of the Kullback–Leibler divergence [Beck and Teboulle, 2003]. It was shown in Korba and Portier [2022] that \mathcal{F}_e satisfies the contraction property (1) with $\rho = 1 - \varepsilon$. The parameter ε thus controls a trade-off between the speed of convergence and the discrepancy between successive iterates.

From Jensen’s inequality, it also holds that

$$\text{KL}(\mu \parallel \mathcal{F}_e(\mu)) \leq \varepsilon \text{KL}(\mu \parallel \pi),$$

which shows that consecutive iterates remain close when ε is small. This observation is central in practice, as it impacts the quality of Monte Carlo approximations of the mapping.

2.3 Limitations of Entropic Mirror Descent

Although the Entropic Mirror Descent mapping enjoys strong theoretical guarantees, it is generally intractable for sampling and density evaluation. Practical implementations therefore rely on Monte Carlo approximations of $\mathcal{F}_e(\mu)$, typically based on weighted samples drawn from μ . As in importance sampling, the quality of these approximations heavily depends on the overlap between μ and π .

In multimodal settings, when the current iterate μ_t fails to cover certain regions of high probability mass under π , Monte Carlo approximations of $\mathcal{F}_e(\mu_t)$ may entirely miss these regions. As a consequence, the resulting approximate sequence may fail to converge to π . This phenomenon persists even when the variational family is sufficiently rich, as illustrated in Figure 1. The target distribution is set to a univariate Gaussian mixture with two components and the initial proposal μ_0 to a mixture with its two modes at 0. In this setting, the sequence $\{\mu_t\}_{t \geq 0}$ can be exactly computed and we indeed observe that it converges to π . However, when replacing the mapping \mathcal{F}_e by its Monte Carlo counterpart, the update resume to sampling from the current proposal distribution and the method fails to visit the second mode.

These limitations motivate the introduction of additional mechanisms that explicitly promote exploration of the state space. In particular, it is natural to consider Markov transition kernels that are able to move samples into regions that are unlikely under the current proposal but relevant under the target distribution. This idea follows recent works such as [Samsonov et al. \[2022\]](#) which design non-local moves and global proposals to improve sampling performance of MCMC algorithms or [Cabezas et al. \[2024\]](#) where the authors proposed an adaptive MCMC scheme combining a non-local, flow-informed transition kernel and a local transition kernel, which generate samples from a sequence of annealed target distributions.

3 Entropic Mirror Monte Carlo

3.1 Mapping with invariant Markov kernels

To address the aforementioned limitations, we introduce a new mapping that combines importance reweighting with Markovian dynamics. Let K_π be a π -invariant Markov transition kernel. For $0 < \varepsilon \leq 1$ and $0 < \lambda \leq 1$, we define

$$\mathcal{F}_{\text{em}}(\mu; \lambda, K_\pi, \varepsilon) = \lambda \mathcal{F}_e(\mu) + (1 - \lambda) \mathcal{F}_{K_\pi}(\mu), \quad (3)$$

where

$$\mathcal{F}_{K_\pi}(\mu) \propto \left(\frac{d\pi}{d\mu} \right)^\varepsilon \mu K_\pi.$$

The first term preserves the contraction properties of Entropic Mirror Descent and exploits regions already identified by the current proposal. The second term leverages the exploratory power of the Markov kernel and assigns significant weight to samples that reach previously unexplored regions of the target distribution.

[Lemma 1](#) ensures that the mapping (3) is well defined under mild assumptions. Namely, if we have an initial distribution μ_0 which satisfies $\|d\pi/d\mu_0\|_\infty < \infty$, the mapping (3) can define a sequence of probability measure $\{\mu_t\}_{t \in \mathbb{N}}$ given, for $0 < \lambda_{t-1} \leq 1$; $0 < \varepsilon \leq 1$, by

$$\mu_t = \mathcal{F}_{\text{em}}(\mu_{t-1}; \lambda_{t-1}, K_\pi, \varepsilon), \quad (4)$$

since all the iterates μ_t then also satisfy $\|d\pi/d\mu_t\|_\infty < \infty$.

Lemma 1. *Given $0 < \varepsilon \leq 1$ and $0 < \lambda \leq 1$, if $\mu \in \mathbb{M}_\pi$ satisfies*

$$\left\| \frac{d\pi}{d\mu} \right\|_\infty < \infty,$$

then $\mathcal{F}_{\text{em}}(\mu; \lambda, K_\pi, \varepsilon)$ is well defined and is a probability measure in \mathbb{M}_π . Moreover, it satisfies

$$\left\| \frac{d\pi}{d\mathcal{F}_{\text{em}}(\mu; \lambda, K_\pi, \varepsilon)} \right\|_\infty < \infty.$$

[Proposition 1](#) establishes that the contraction property is preserved. This result also establishes that if we have not achieved $\mu_t = \pi$ and set $\varepsilon = 1$, we can always find a sequence $\{\lambda_t\}_{t \in \mathbb{N}}$ such that, for any choice of π -invariant transition kernel K_π , the mapping \mathcal{F}_{em} differs from the original Entropic Mirror Descent transformation (2).

Proposition 1. *Let $0 < \varepsilon \leq 1$ and $\mu_0 \in \mathbb{M}_\pi$ such that $\|d\pi/d\mu_0\|_\infty < \infty$. If K_π is π -invariant, then there exists a sequence $0 < \lambda_t \leq 1$ such that the iterates*

$$\mu_t = \mathcal{F}_{\text{em}}(\mu_{t-1}; \lambda_{t-1}, K_\pi, \varepsilon)$$

satisfy, for all $t \in \mathbb{N}$,

$$\text{KL}(\pi \| \mu_t) \leq (1 - \varepsilon)^t \text{KL}(\pi \| \mu_0).$$

3.2 Mapping with Unadjusted Langevin kernel

Proposition 1 only requires that K_π is π -invariant, so our mapping can be used with various Markov Chain Monte Carlo methods such as Metropolis-adjusted Langevin [Besag, 1994], Hamiltonian Monte Carlo [Neal et al., 2011] or iSIR [Andrieu et al., 2010] algorithms.

In practice, however, Markov kernels that are not π -invariant may exhibit strong exploratory properties. A prominent example is the Unadjusted Langevin Algorithm, [see for instance Durmus and Moulines, 2019] and the references therein. This Markov Chain Monte Carlo algorithm is deduced from the Euler-Maruyama discretization of the Langevin diffusion which yields the iterates:

$$X_{k+1} = X_k + \gamma \nabla \log \pi(X_k) + \sqrt{2\gamma} Z_{k+1},$$

where $(Z_k)_{k \geq 1}$ is an i.i.d. sequence of d -dimensional standard Gaussian vectors and γ is a fixed positive step-size. We denote by R_γ the Markov kernel associated with a single step of the Unadjusted Langevin Algorithm with step size $\gamma > 0$. For all $x \in \mathbb{R}^d$, $R_\gamma(x, \cdot)$ is the Gaussian distribution with mean $x + \gamma \nabla \log \pi(x)$ and covariance matrix $2\gamma I_d$. Although R_γ does not admit π as invariant distribution, it is known to possess a unique invariant distribution, denoted by π_γ , under suitable regularity assumptions.

Condition 3.1. The target distribution π satisfies a log-Sobolev inequality: there exists a constant $C_{\text{LS}} > 0$ such that for all smooth functions $g : \mathbb{R}^d \rightarrow \mathbb{R}$,

$$\text{Ent}_\pi(g^2) = \int g^2 \log \frac{g^2}{\int g^2 d\pi} d\pi \leq C_{\text{LS}} \int \|\nabla g\|^2 d\pi.$$

Condition 3.2. The log-density of the target distribution is continuously differentiable and L -smooth: there exists a constant $L > 0$ such that for all $x, y \in \mathbb{R}^d$,

$$\|\nabla \log \pi(x) - \nabla \log \pi(y)\| \leq L \|x - y\|.$$

Conditions 3.1 and 3.2 are standard in the sampling literature [Durmus and Moulines, 2019, Vempala and Wibisono, 2019, Chewi et al., 2022, Erdogdu et al., 2022]. In particular, Condition 3.1 provides a powerful tool for analyzing the exponential convergence of Markov semi-groups [Bakry et al., 2014]. This condition holds for a large class of probability measures, including log-concave distributions and is stable under bounded perturbations [Holley and Stroock, 1987].

Condition 3.3. There exist a measurable function $V : \mathbb{R}^d \rightarrow [1, +\infty)$, a constant $b \geq 0$, and a compact set $C \subset \mathbb{R}^d$ such that

$$R_\gamma V \leq V - 1 + b \mathbb{1}_C. \quad (5)$$

Condition 3.3 ensures the existence of an invariant distribution π_γ for R_γ [Meyn and Tweedie, 2012]. Using only Condition 3.2, it is easily shown that for any compact set $K \subset \mathbb{R}^d$ there exists $C \geq 0$ such that for all $x \in K$ and $A \in \mathcal{B}(\mathbb{R}^d)$

$$R_\gamma(x, A) \geq C_K \text{Leb}(A \cap K), \quad (6)$$

and thus R_γ is Leb-irreducible and strongly aperiodic. Therefore, following Theorem 14.0.1 of Meyn and Tweedie [2012], R_γ is positive recurrent and admits a unique invariant distribution if and only if (5) is satisfied for some petite set C . In Condition 3.3, we only strengthen this condition on C and suppose that it is compact which is satisfied in most applications.

We consider the sequence of probability measures $\{\mu_t^R\}_{t \in \mathbb{N}} \subset \mathbb{M}_\pi$ defined recursively, for $t \geq 1$, by

$$\mu_t^R = \mathcal{F}_{\text{em}}(\mu_{t-1}^R; \lambda_{t-1}, R_\gamma, \varepsilon),$$

with initial distribution $\mu_0^R \in \mathbb{M}_\pi$.

Algorithm 1 Entropic Mirror Monte Carlo (EM2C)

Input: number of iterations T , number of samples N , initial distribution μ_0 , parameters $0 < \varepsilon \leq 1$, $0 < \lambda_t \leq 1$ ($0 \leq t \leq T - 1$), Markov kernel K .

Output: proposal distribution $\tilde{\mu}_T$.

for $t = 0$ **to** $T - 1$ **do**

- Sample $X_t^{1:N} \sim \tilde{\mu}_t^{\otimes N}$.
- Sample $Y_t^{1:N} \sim K(X_t^1, \cdot) \otimes \cdots \otimes K(X_t^N, \cdot)$.
- for** $i = 1$ **to** N **do**

 - Compute
$$\omega_t^i \propto \left\{ \frac{d\pi}{d\tilde{\mu}_t}(X_t^i) \right\}^\varepsilon, \quad \varpi_t^i \propto \left\{ \frac{d\pi}{d\tilde{\mu}_t}(Y_t^i) \right\}^\varepsilon.$$

- end for**
- for** $i = 1$ **to** N **do**

 - Sample
$$Z_t^i \sim \widehat{\mathcal{F}}_{\tilde{\mu}_t}^N = \lambda_t \sum_{j=1}^N \omega_t^j \delta_{X_t^j} + (1 - \lambda_t) \sum_{j=1}^N \varpi_t^j \delta_{Y_t^j}.$$

- end for**
- Compute
$$\tilde{\mu}_{t+1} = \underset{\mu_\theta \in \mathcal{F}_\theta}{\operatorname{argmin}} \mathcal{R}(\widehat{\mathcal{F}}_{\tilde{\mu}_t}^N, \mu_\theta).$$

end for

Theorem 2. Assume that Conditions 3.1, 3.2, and 3.3 hold. Let $\mu_0^R \in \mathbb{M}_\pi$ satisfy $\|d\pi/d\mu_0^R\|_\infty < \infty$. Then, there exists a sequence $0 < \lambda_t \leq 1$ such that

$$\|\pi - \mu_t^R\|_{\text{TV}} \leq (1 - \varepsilon)^{t/2} \sqrt{2 \text{KL}(\pi_\gamma \parallel \mu_0^R)} + 4\sqrt{2\gamma dL^2 C_{\text{LS}}}.$$

Theorem 2 shows that, although the Unadjusted Langevin kernel introduces a bias through its invariant distribution π_γ , this bias remains controlled, while the contraction induced by the Entropic Mirror component is preserved.

3.3 Monte Carlo implementation: the EM2C algorithm

As with the entropic mirror mapping, in most settings the mapping \mathcal{F}_{em} is intractable and can only be accessed through samples. The theoretical sequence $(\mu_t)_{t \in \mathbb{N}}$ as defined in (4) is thus replaced by a sequence of surrogate distributions $(\tilde{\mu}_t)_{t \in \mathbb{N}}$. The resulting Monte Carlo procedure is summarized in Algorithm 1. Namely, given the current proposal, say $\tilde{\mu}_t$, we sample $(X_t^{1:N})$ from $\tilde{\mu}_t$ and propagate them through a Markov kernel $(Y_t^{1:N})$, which yields the empirical distribution

$$\widehat{\mathcal{F}}_{\tilde{\mu}_t}^N = \lambda_t \sum_{i=1}^N \omega_t^i \delta_{X_t^i} + (1 - \lambda_t) \sum_{i=1}^N \varpi_t^i \delta_{Y_t^i}.$$

The surrogate distribution is then computed as the minimizer of a loss function \mathcal{R} between $\mu_\theta \in \mathcal{F}_\theta$, where \mathcal{F}_θ is a family of parametric probability distributions, and the empirical measure $\widehat{\mathcal{F}}_{\tilde{\mu}_t}^N$.

The projection onto \mathcal{F}_θ can be achieved in several ways. We begin by describing two common situations, both of which consist to choosing \mathcal{R} as the Kullback–Leibler, and minimizing, with respect to θ , the Kullback–Leibler divergence between the sample distribution and the distribution μ_θ .

Mixture models and EM algorithm. In the case where F_θ is assumed to be a family of mixture models with base probability distributions $\{f_{\eta_k} ; 1 \leq k \leq K\}$, we have:

$$\mathsf{F}_\theta = \left\{ \sum_{k=1}^K p_k f_{\eta_k} ; \sum_{k=1}^K p_k = 1, p_k \geq 0 \right\}.$$

Estimation is typically carried out via the Expectation Maximization (EM) algorithm, which produces a sequence of parameter estimates by maximizing approximately the loglikelihood function:

$$\mathcal{R}(\widehat{\mathcal{F}}_{\tilde{\mu}_t}^N, \mu_\theta) = \sum_{i=1}^N \log \left(\sum_{k=1}^K p_k f_{\eta_k}(Z_t^i) \right),$$

where $Z_t^{1:N}$ are samples from $\widehat{\mathcal{F}}_{\tilde{\mu}_t}^N$.

Normalizing flows. In recent years, several works have introduced hybrid methods which combine normalizing flows with MCMC algorithms to enhance sampling performance [Gabrié et al. \[2022\]](#), [Grenioux et al. \[2023\]](#). Normalizing flows aim at learning a flexible parametric distribution from $Z_t^{1:N} \sim \widehat{\mathcal{F}}_{\tilde{\mu}_t}^N$ by constructing an invertible and differentiable transformation that maps a simple base distribution to the distribution of $Z_t^{1:N}$. Consider a family of bijective mappings $f_\theta : \mathbb{R}^d \rightarrow \mathbb{R}^d$ parameterized by $\theta \in \Theta$, such that a random variable Z drawn from a tractable base density p_Z is transformed into $X = f_\theta(Z)$, with induced density given by the change-of-variables formula

$$p_\theta(x) = p_Z(f_\theta^{-1}(x)) |\det Df_\theta^{-1}(x)|,$$

where Df_θ^{-1} is the Jacobian of f_θ^{-1} . Therefore,

$$\mathsf{F}_\theta = \{x \mapsto p_Z(f_\theta^{-1}(x)) |\det Df_\theta^{-1}(x)| ; \theta \in \Theta\}.$$

and the loglikelihood objective is then given by

$$\mathcal{R}(\widehat{\mathcal{F}}_{\tilde{\mu}_t}^N, \mu_\theta) = \sum_{i=1}^N \log p_\theta(Z_t^i),$$

which can be equivalently expressed as

$$\mathcal{R}(\widehat{\mathcal{F}}_{\tilde{\mu}_t}^N, \mu_\theta) = \sum_{i=1}^n \log p_Z(f_\theta^{-1}(Z_t^i)) + \sum_{i=1}^n \log |\det Df_\theta^{-1}(Z_t^i)|.$$

While the ideal mapping \mathcal{F}_{em} enjoys explicit contraction properties, these guarantees do not generally extend to the projected sequence $(\tilde{\mu}_t)_{t \in \mathbb{N}}$ used in practice. The projection onto a parametric family introduces an approximation error that depends on the expressiveness of F_θ and on the numerical procedure employed, which may weaken or break the contraction. Nevertheless, our experiments show that the resulting algorithm remains stable and effective in practice.

4 Numerical study

In this section, we present numerical experiments assessing the performance of Algorithm 1 on multimodal target distributions. We evaluate mode recovery, the effect of the mixing parameter λ and the exploration kernel, and the discrepancy between the learned proposal $\tilde{\mu}_T$ and the target distribution π using the sliced Wasserstein distance (Appendix D.1).

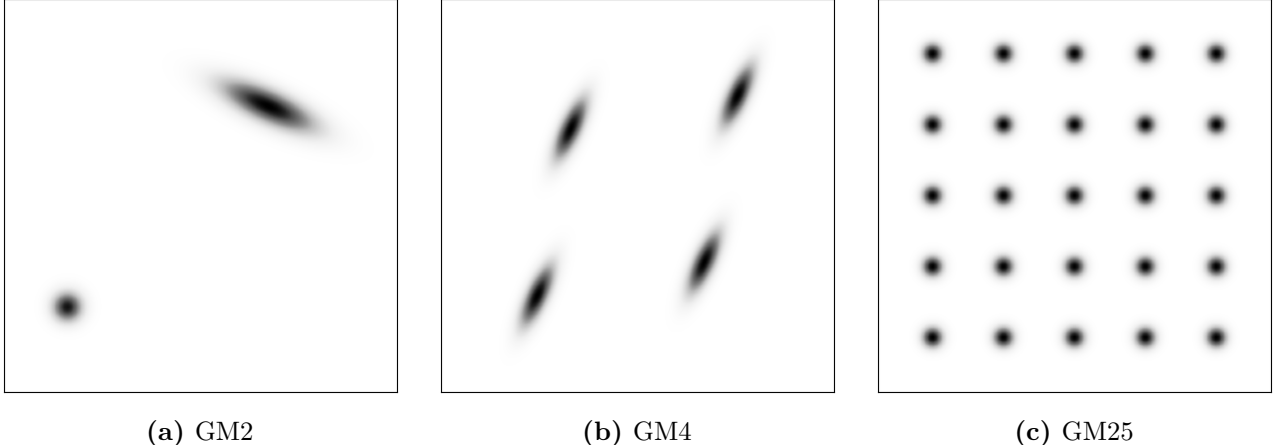


Figure 2: Marginal Gaussian mixture distribution $\tilde{\pi}_i$ associated with the benchmark target distributions $\pi_{i,d}$ as defined in (7).

4.1 Multidimensional Gaussian mixture benchmarks

Target distributions. We consider a family of high-dimensional targets build as a tensor product of one of the following two-dimensional Gaussian mixture models (see Figure 2).

- **GM2 (two-component, unbalanced)**

$$\tilde{\pi}_1 = 0.2\mathcal{N}(\mathbf{0}_2, I_2) + 0.8\mathcal{N}\left(\begin{bmatrix} 20 \\ 20 \end{bmatrix}, \begin{bmatrix} 10 & -4 \\ -4 & 3 \end{bmatrix}\right).$$

- **GM4 (four-component, anisotropic)**

$$\tilde{\pi}_2 = 0.25 \sum_{j=1}^4 \mathcal{N}\left(m_j, \begin{bmatrix} 3 & 4 \\ 4 & 10 \end{bmatrix}\right),$$

with $m_1 = (-10, 10)^\top$, $m_2 = (10, -10)^\top$, $m_3 = (15, 15)^\top$, and $m_4 = (-15, -15)^\top$.

- **GM25 (twenty-five-component, isotropic)**

$$\tilde{\pi}_3 = 0.2 \sum_{\ell=0}^4 \sum_{k=0}^4 \mathcal{N}\left(\begin{bmatrix} 5\ell \\ 5k \end{bmatrix}, 0.25I_2\right).$$

Given an even dimension d and a mixture distribution $\tilde{\pi}_i$, the target writes as

$$\pi_{i,d} = \tilde{\pi}_i^{\otimes d/2}, \quad i = 1, 2, 3. \quad (7)$$

Experimental design. In all experiments, the initial proposal is a Gaussian distribution

$$\mu_0 = \mathcal{N}(30\mathbf{1}_d, I_d),$$

placing the initial mass in a low-probability region of the target and providing a common, challenging initialization across all models.

The variational family F_θ is chosen as a tensorized Gaussian mixture model, and the projection step is implemented via an expectation–maximization (EM) algorithm. Implementation details, including the structure of the variational family and EM hyperparameters, are provided in Appendix B.4.

Algorithm 1 is run with $\varepsilon = 0.8$, $N = 2,000$ particles per iteration, and constant mixing parameters $\lambda \in \{0.5, 0.8, 1.0\}$. The number of EM2C iterations T and the parameters of the exploration kernel K are tuned to the target model and the ambient dimensions d to account for differences in scale and geometry of the target π .

For each setting, the exploration kernel K is chosen either as a π -invariant Random Walk (RW) Metropolis kernel, with variance parameter σ_K^2 , or as the Unadjusted Langevin Algorithm (ULA), with step size γ_K . At each EM2C iteration, the selected kernel is applied for a fixed number of n_K steps. Complete kernel configurations and experimental settings for all targets and dimensions are given in Appendix B.5.

Results. Figure 3 illustrates the evolution of the proposal distribution obtained with Algorithm 1 with respect to the GM4 target in dimension $d = 10$. For each value of λ , we compare the behaviour of EM2C using RW or ULA kernel. Figure 3 shows the impact of both the mixing parameter and the exploration kernel on the preservation of multimodality: smaller values of λ promote exploration and help maintaining multiple modes, while larger values may result in mode imbalance when exploration is insufficient. Additional qualitative evolution plots for the other mixture targets and dimensions are provided in Appendix B.2. Overall, the ULA kernel consistently outperforms the RW kernel, as the latter may suffer from frequent rejections in low-density regions, whereas ULA leverages gradient information to guide proposals toward regions of high target density.

This qualitative behaviour is further reflected in the evolution of the sliced Wasserstein distance across EM2C iterations. For the GM4 benchmark with $d = 10$, Figure 4 shows that smaller values of λ lead to a rapid reduction of the discrepancy between the proposal and the target, whereas $\lambda = 1$ results in poor convergence. Final sliced Wasserstein distances at convergence for the GM4 benchmark with dimensions $d = 10$ and $d = 20$ are reported in Table 1. Additional sliced Wasserstein results for the other targets and dimensions are provided in Appendix B.1.

We further compare EM2C with a standard Markov chain Monte Carlo sampler using similar local dynamics and a matched computational budget for the GM4 benchmark in dimension $d=10$ (details and results given in Appendix B.3).

4.2 Multimodal Targets with Complex Geometry

We further assess the performance of EM2C on a collection of target distributions exhibiting strong multimodality and nontrivial geometry. Such benchmarks are commonly used to stress-test sampling algorithms, as they combine disconnected modes, curved supports, and regions of low probability that hinder exploration.

Table 1: Final sliced Wasserstein distances for the GM4 benchmark with dimensions $d = 10$ and 20 , using Random Walk (RW) or Unadjusted Langevin Algorithm (ULA) kernels. We report the mean \pm standard deviation over three independent runs.

d	λ	RW	ULA
10	1.0	20.60 ± 0.40	20.41 ± 1.07
	0.8	4.42 ± 2.64	0.81 ± 0.17
	0.5	2.09 ± 1.80	0.84 ± 0.03
20	1.0	24.50 ± 1.08	23.28 ± 0.70
	0.8	7.82 ± 0.52	5.37 ± 0.68
	0.5	1.81 ± 0.58	3.13 ± 0.72

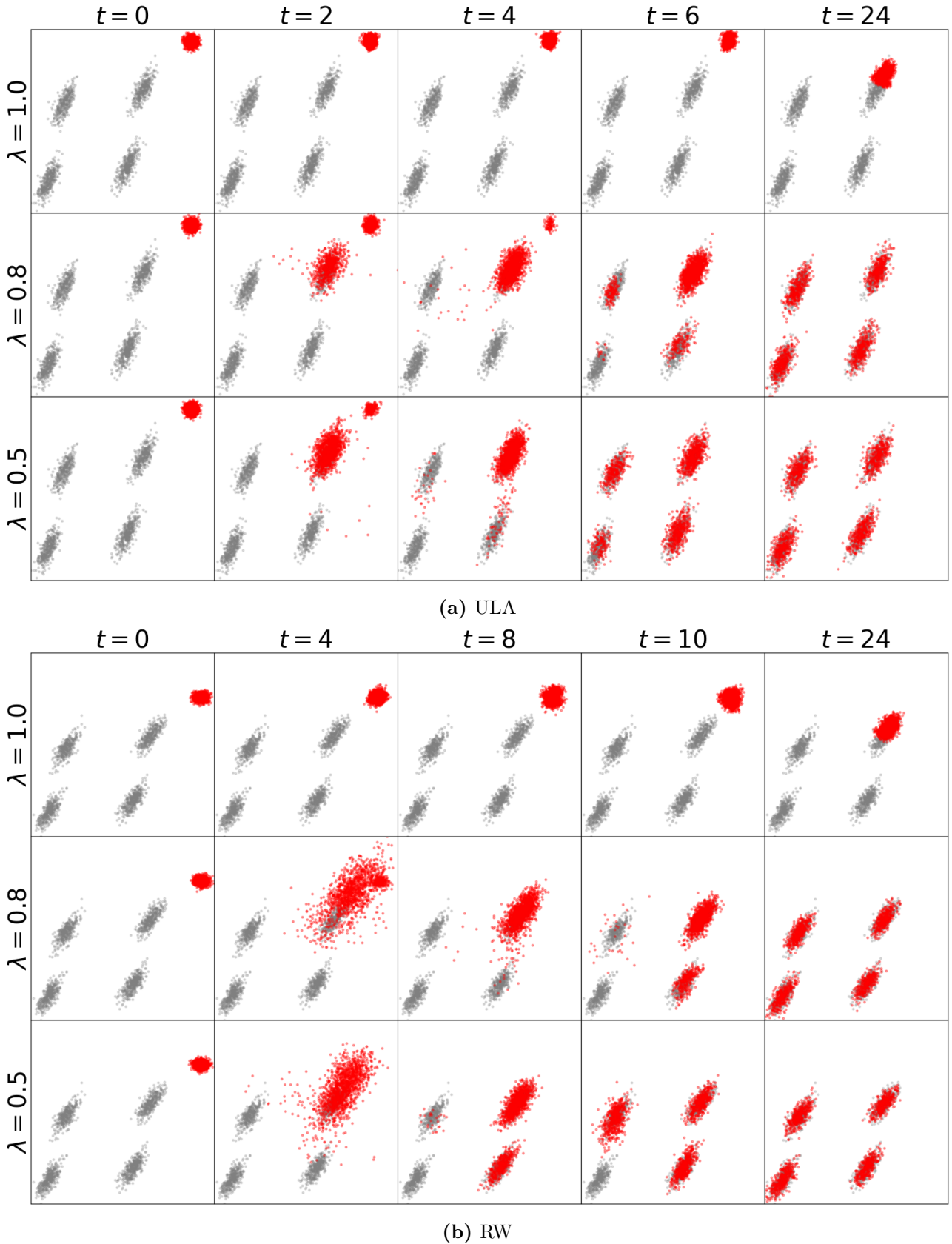


Figure 3: Evolution of EM2C proposal distributions for the GM4 target in dimension $d = 10$. Rows correspond to $\lambda \in \{0.5, 0.8, 1.0\}$, columns to EM2C iterations. For visualization, we display the two-dimensional projection onto coordinates (x_0, x_1) . Gray and red points denote samples from π and $\tilde{\mu}_t$, respectively.

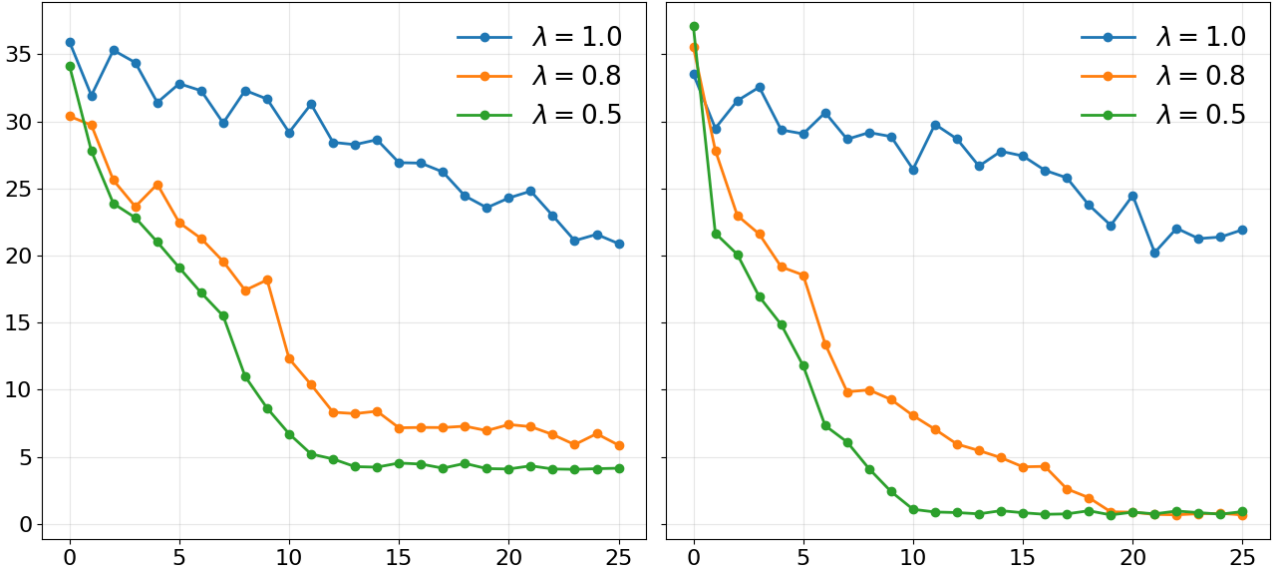


Figure 4: Evolution of $SW_2(\mu_t, \pi)$ for the GM4 target ($d = 10$), shown for RW and ULA kernels and $\lambda \in \{0.5, 0.8, 1.0\}$.

Target distributions. We study the following target distributions on \mathbb{R}^2 .

- **Dual Moons:** two interleaving half-circles with additive Gaussian noise. For $x = (x_1, x_2)$, $(a, b) = (0.09, 0.08)$

$$\pi(x) = (1 + e^{4x_1/a}) \exp\left\{-\frac{(\|x\| - 1)^2}{b} - \frac{(x_1 - 2)^2}{2a}\right\}.$$

- **Two Rings:** two concentric annular distributions with different radii. For $\sigma = 0.1$,

$$\pi(x) = \frac{1}{\|x\|} \sum_{k \in \{1, 4\}} \exp\left(-\frac{(\|x\| - k)^2}{2\sigma^2}\right).$$

Experimental design. We evaluate EM2C under challenging initializations, where the initial distribution places little or no mass on the target support or covers only a subset of the modes. Such initializations are representative of practical scenarios in which prior information is limited or misspecified. While initializing from a broad distribution already covering the target may allow standard samplers to perform well, this setting masks the intrinsic exploration difficulties posed by multimodal targets. Our goal is therefore to highlight regimes where exploration is critical and where the combination of entropic reweighting and Markovian dynamics in EM2C provides a tangible advantage.

In Algorithm 1, the projection step is achieved using normalizing flows as the variational family \mathcal{F}_θ (see Appendix C.2 for details).

We compare EM2C against (i) Random Walk MCMC Sampler (RW), (ii) the No-U-Turn Sampler (NUTS), and (iii) Annealed Importance Sampling (AIS). All methods are implemented under a common experimental protocol and allocated comparable computational budgets. For a given target, the same initial distribution and the same number of particles ($N = 10,000$) are used across all compared methods, ensuring a fair comparison. Complete specifications of the initial distributions, and method-specific hyperparameters are provided in Appendix C.3.

Results. Figure 5 presents qualitative density estimates obtained by each method at convergence. Under the challenging initialization considered here, the behaviour of the compared

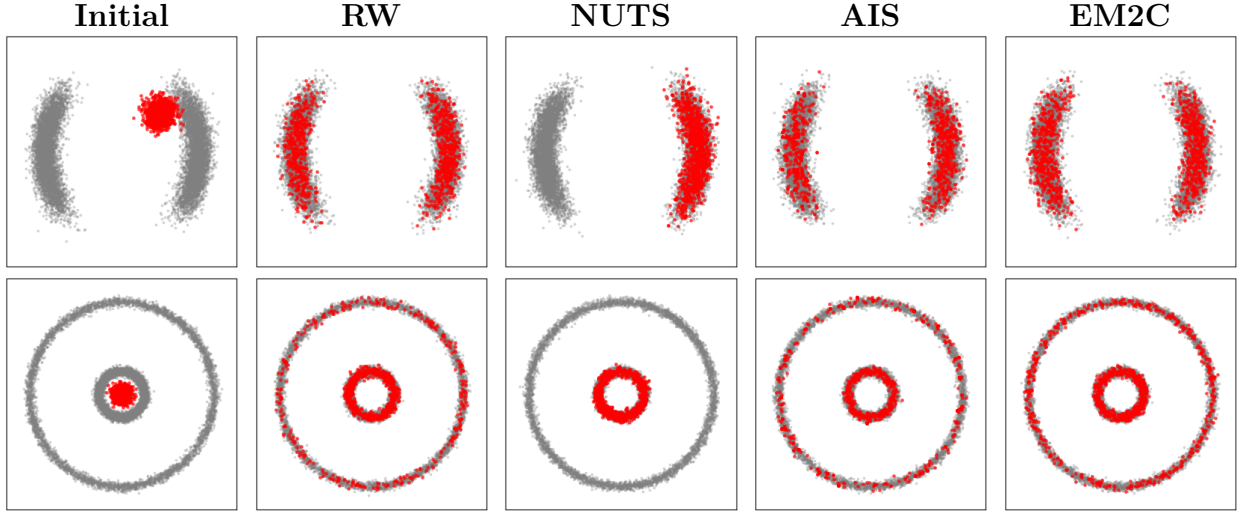


Figure 5: Qualitative comparison of sampling methods on Two-dimensional multimodal targets (top row: dual moons, bottom row: two rings). Gray points denote samples from the target distribution.

methods differs markedly. The Random-Walk MCMC sampler is able to partially recover the multimodal structure of the target, with a subset of particles reaching the secondary mode. In contrast, NUTS typically concentrates on a single mode in this setting and fails to explore the full target support. Annealed Importance Sampling exhibits a strong dependence on the initialization: with the initialization used in our experiments, AIS only partially recovers the secondary mode, while broader initial proposals can lead to improved mode coverage. In comparison, EM2C consistently recovers all target modes under the same initialization and using the same step size as RW and AIS, highlighting the benefit of delayed reweighting combined with explicit exploration steps. Additional qualitative results illustrating the evolution of EM2C proposals on two-dimensional benchmarks are provided in Appendix C.

These qualitative observations are corroborated by quantitative evaluations based on both the sliced Wasserstein distance and the energy distance (see Appendix D.2 for definition and computation). Table 2 reports the final $SW_2(\mu_T, \pi)$ and $ED(\mu_T, \pi)$ values for all considered datasets and methods. EM2C achieves systematically lower discrepancies under challenging initialization regimes, confirming its improved ability to explore complex target geometries.

When initialized from a sufficiently broad proposal covering the target support, the performance gap between methods narrows, as exploration becomes less critical. In the more challenging and practically relevant settings considered here, EM2C nevertheless exhibits superior robustness to initialization and improved mode recovery.

Table 2: Quantitative comparison on two-dimensional benchmarks. Lower values indicate better agreement with the target distribution. We report the mean \pm standard deviation over three runs.

(a) Dual Moons				(b) Two Rings				
	RW	NUTS	AIS		RW	NUTS	AIS	
SW_2	0.62 ± 0.01	1.74 ± 0.05	0.17 ± 0.08	0.071 ± 0.016	0.55 ± 0.01	1.42 ± 0.001	0.65 ± 0.18	0.049 ± 0.008
ED	0.082 ± 0.011	1.48 ± 0.01	0.005 ± 0.003	0.0004 ± 0.0001	0.056 ± 0.002	0.441 ± 0.001	0.141 ± 0.067	0.0006 ± 0.0002

5 Discussion

In this paper, we propose a new algorithm to build sequentially proposal distributions combining a contractive entropic mirror descent step with an exploratory Markov kernel component. When using the Unadjusted Langevin kernel, we show that the bias induced by the remains controlled and does not hinder convergence, while preserving the contraction properties of the method. We also introduce an importance sampling scheme to approximate the idealized algorithm and demonstrate its effectiveness numerically. The main limitations and directions for future work include the deployment of the method in challenging very high-dimensional settings, notably with deep learning architectures, and the theoretical analysis of contraction properties for the Monte Carlo procedure.

References

S. Agapiou, O. Papaspiliopoulos, D. Sanz-Alonso, and A. M. Stuart. Importance sampling: Intrinsic dimension and computational cost. *Statistical Science*, pages 405–431, 2017.

C. Andrieu, A. Doucet, and R. Holenstein. Particle Markov chain Monte Carlo methods. *J. R. Stat. Soc. Ser. B Stat. Methodol.*, 72(3):269–342, 2010.

D. Bakry, I. Gentil, M. Ledoux, et al. *Analysis and geometry of Markov diffusion operators*, volume 103. Springer, 2014.

A. Beck and M. Teboulle. Mirror descent and nonlinear projected subgradient methods for convex optimization. *Operations Research Letters*, 31(3):167–175, 2003.

J. Besag. Comments on “Representations of knowledge in complex systems” by U. Grenander and M. Miller. *J. Roy. Statist. Soc. Ser. B*, 56:591–592, 1994.

A. Cabezas, L. Sharrock, and C. Nemeth. Markovian flow matching: Accelerating mcmc with continuous normalizing flows. *Advances in Neural Information Processing Systems*, 37: 104383–104411, 2024.

O. Cappé, A. Guillin, J.-M. Marin, and C. P. Robert. Population Monte Carlo. *Journal of Computational and Graphical Statistics*, 13(4):907–929, 2004.

S. Chatterjee and P. Diaconis. The sample size required in importance sampling. *The Annals of Applied Probability*, 28(2):1099–1135, 2018.

S. Chewi, M. A. Erdogdu, M. Li, R. Shen, and S. Zhang. Analysis of Langevin Monte Carlo from Poincare to Log-Sobolev. In P.-L. Loh and M. Raginsky, editors, *Proceedings of Thirty Fifth Conference on Learning Theory*, volume 178 of *Proceedings of Machine Learning Research*, pages 1–2. PMLR, 02–05 Jul 2022. URL <https://proceedings.mlr.press/v178/chewi22a.html>.

J.-M. Cornuet, J.-M. Marin, A. Mira, and C. P. Robert. Adaptive Multiple Importance Sampling. *Scandinavian Journal of Statistics*, 39(4):798–812, 2012.

B. Dai, N. He, H. Dai, and L. Song. Provable Bayesian Inference via Particle Mirror Descent. In *Proceedings of the 19th International Conference on Artificial Intelligence and Statistics*, volume 51, pages 985–994. PMLR, 09–11 May 2016.

K. Daudel, R. Douc, and F. Portier. Infinite-dimensional gradient-based descent for alpha-divergence minimisation. *The Annals of Statistics*, 49(4):2250–2270, 2021.

A. Durmus and É. Moulines. High-dimensional Bayesian inference via the unadjusted Langevin algorithm. *Bernoulli*, 25(4A):2854 – 2882, 2019. doi: 10.3150/18-BEJ1073. URL <https://doi.org/10.3150/18-BEJ1073>.

M. A. Erdogdu, R. Hosseinzadeh, and S. Zhang. Convergence of langevin monte carlo in chi-squared and rényi divergence. In *International Conference on Artificial Intelligence and Statistics*, pages 8151–8175. PMLR, 2022.

M. Gabrié, G. M. Rotskoff, and E. Vanden-Eijnden. Adaptive Monte Carlo augmented with normalizing flows. *Proceedings of the National Academy of Sciences*, 119(10):e2109420119, 2022.

L. Grenioux, A. Durmus, É. Moulines, and M. Gabrié. On sampling with approximate transport maps. *arXiv preprint arXiv:2302.04763*, 2023.

L. Grenioux, M. Noble, and M. Gabrié. Improving the evaluation of samplers on multi-modal targets. *arXiv preprint arXiv:2504.08916*, 2025.

R. Holley and D. W. Stroock. Logarithmic Sobolev inequalities and stochastic Ising models. *Journal of Statistical Physics*, 46(5):1159–1194, 1987.

A. Korba and F. Portier. Adaptive Importance Sampling meets Mirror Descent : a Bias-variance Tradeoff. In *Proceedings of The 25th International Conference on Artificial Intelligence and Statistics*, volume 151, pages 11503–11527. PMLR, 2022.

S. P. Meyn and R. L. Tweedie. *Markov chains and stochastic Stability*. Springer London, 2012.

R. M. Neal et al. *MCMC using Hamiltonian dynamics*, chapter 5 (Handbook of Markov Chain Monte Carlo). Chapman and Hall/CRC, 2011.

M.-S. Oh and J. O. Berger. Integration of Multimodal Functions by Monte Carlo Importance Sampling. *Journal of the American Statistical Association*, 88(422):450–456, 1993.

G. O. Roberts and J. S. Rosenthal. General state space markov chains and mcmc algorithms. *Probability surveys*, 1:20–71, 2004.

S. Samsonov, E. Lagutin, M. Gabrié, A. Durmus, A. Naumov, and E. Moulines. Local-Global MCMC kernels: the best of both worlds. In *Advances in Neural Information Processing Systems*, volume 35, pages 5178–5193, 2022.

T. Van Erven and P. Harremos. Rényi divergence and kullback-leibler divergence. *IEEE Transactions on Information Theory*, 60(7):3797–3820, 2014.

S. Vempala and A. Wibisono. Rapid Convergence of the Unadjusted Langevin Algorithm: Isoperimetry Suffices. In *Advances in Neural Information Processing Systems*, volume 32, 2019.

Appendix

A Proofs

A.1 Proof of Lemma 1

If $\|\mathrm{d}\pi/\mathrm{d}\mu\|_\infty < \infty$ then

$$\int \left(\frac{\mathrm{d}\pi}{\mathrm{d}\mu} \right)^\varepsilon \mathrm{d}\mu K_\pi < \infty;$$

so $\mathcal{F}_{\text{em}}(\mu; \lambda, K_\pi, \varepsilon)$ is indeed a probability measure. Next, since $0 \leq \varepsilon \leq 1$ and $0 < \lambda \leq 1$, we have that

$$\sup_{x \in \mathbb{R}^d} \frac{\mathrm{d}\pi}{\mathrm{d}\mathcal{F}_{\text{em}}(\mu; \lambda, K_\pi, \varepsilon)}(x) \leq \sup_{x \in \mathbb{R}^d} \left\{ \frac{1}{\lambda} \frac{\mathrm{d}\pi}{\mathrm{d}\mu}(x)^{1-\varepsilon} \int \frac{\mathrm{d}\pi}{\mathrm{d}\mu}(y)^\varepsilon \mu(\mathrm{d}y) \right\} < \infty.$$

A.2 Proof of Proposition 1

For any sequence $0 < \lambda_t \leq 1$, $t \in \mathbb{N}$, the convexity of the Kullback-Leibler divergence leads to

$$\begin{aligned} \mathsf{KL}(\pi \parallel \mu_{t+1}) &\leq \lambda_t \mathsf{KL}(\pi \parallel \mathcal{F}_e(\mu_t)) + (1 - \lambda_t) \mathsf{KL}(\pi \parallel \mathcal{F}_{K_\pi}(\mu_t)) \\ &\leq \lambda_t (1 - \varepsilon) \mathsf{KL}(\pi \parallel \mu_t) + (1 - \lambda_t) \{ \mathsf{KL}(\pi \parallel \mu_t K_\pi) - \varepsilon \mathsf{KL}(\pi \parallel \mu_t) \} \\ &\quad + \lambda_t \log \int f_t^\varepsilon \mathrm{d}\mu_t + (1 - \lambda_t) \log \int f_t^\varepsilon \mathrm{d}\mu_t K_\pi, \end{aligned}$$

where f_t stands for the Radon-Nikodym derivative of π with respect to μ_t . The Data Processing inequality of [Van Erven and Harremos \[2014\]](#) combined with the π invariance for K_π yield

$$\mathsf{KL}(\pi \parallel \mu_t K_\pi) = \mathsf{KL}(\pi K_\pi \parallel \mu_t K_\pi) \leq \mathsf{KL}(\pi \parallel \mu_t),$$

and so

$$\mathsf{KL}(\pi \parallel \mu_{t+1}) \leq (1 - \varepsilon) \mathsf{KL}(\pi \parallel \mu_t) + \lambda_t \log \int f_t^\varepsilon \mathrm{d}\mu_t + (1 - \lambda_t) \log \int f_t^\varepsilon \mathrm{d}\mu_t K_\pi.$$

Hence, any sequence $\{\lambda_t\}_{t \in \mathbb{N}}$ such that, for all $t \in \mathbb{N}$

$$\lambda_t \log \int f_t^\varepsilon \mathrm{d}\mu_t + (1 - \lambda_t) \log \int f_t^\varepsilon \mathrm{d}\mu_t K_\pi \leq 0 \tag{8}$$

ensures the contraction. Let $0 < \beta \leq 1$ and consider the sequence

$$\lambda_t = \begin{cases} \frac{\log \int f_t^\varepsilon \mathrm{d}\mu_t K_\pi}{\log \int f_t^\varepsilon \mathrm{d}\mu_t K_\pi - \log \int f_t^\varepsilon \mathrm{d}\mu_t} & \text{if } \log \int f_t^\varepsilon \mathrm{d}\mu_t K_\pi > 0, \\ \beta & \text{otherwise.} \end{cases} \tag{9}$$

This sequence takes values between 0 and 1. Indeed, Jensen's inequality yields that $\int f_t^\varepsilon \mathrm{d}\mu_t \leq 1$, with equality solely if $\mu_t = \pi$ or $\varepsilon = 1$. Therefore, λ_t is also less or equal to 1 when $\log \int f_t^\varepsilon \mathrm{d}\mu_t K_\pi > 0$. The results thus follows since the sequence (9) satisfies condition (8).

A.3 Proof of Theorem 2

Similary to the sequence (9) in the proof of Proposition 1, define

$$\lambda_t^* = \begin{cases} \frac{\log \int f_t^\varepsilon \mathrm{d}\mu_t K_\pi}{\log \int f_t^\varepsilon \mathrm{d}\mu_t K_\pi - \log \int f_t^\varepsilon \mathrm{d}\mu_t} & \text{if } \log \int f_t^\varepsilon \mathrm{d}\mu_t K_\pi > 0, \\ \beta_t & \text{otherwise.} \end{cases} \tag{10}$$

Recall that f_t is the Radon-Nikodym derivative of π with respect to μ_t^R . The convexity of the Kullback-Leibler divergence and the definition of λ_t^* in (10) yield

$$\begin{aligned} \text{KL}(\pi_\gamma \parallel \mu_{t+1}^R) &\leq \lambda_t^* \int \log \frac{d\pi_\gamma}{d f_t^\varepsilon \mu_t^R} d\pi_\gamma + (1 - \lambda_t^*) \int \log \frac{d\pi_\gamma}{d f_t^\varepsilon \mu_t^R R_\gamma} d\pi_\gamma \\ &\quad + \lambda_t^* \log \int f_t^\varepsilon d\mu_t^R + (1 - \lambda_t^*) \log \int f_t^\varepsilon d\mu_t^R R_\gamma \\ &\leq \lambda_t^* \int \log \frac{d\pi_\gamma}{d f_t^\varepsilon \mu_t^R} d\pi_\gamma + (1 - \lambda_t^*) \int \log \frac{d\pi_\gamma}{d f_t^\varepsilon \mu_t^R R_\gamma} d\pi_\gamma. \end{aligned}$$

Next,

$$\begin{aligned} \int \log \frac{d\pi_\gamma}{d f_t^\varepsilon \mu_t^R} d\pi_\gamma &= (1 - \varepsilon) \text{KL}(\pi_\gamma \parallel \mu_t^R) + \varepsilon \text{KL}(\pi_\gamma \parallel \pi), \\ \int \log \frac{d\pi_\gamma}{d f_t^\varepsilon \mu_t^R R_\gamma} d\pi_\gamma &\leq (1 - \varepsilon) \text{KL}(\pi_\gamma \parallel \mu_t^R) + \varepsilon \text{KL}(\pi_\gamma \parallel \pi), \end{aligned}$$

where the second inequality follows using the Data Processing inequality [Van Erven and Harremos, 2014] and the fact that R_γ is π_γ -invariant. Thus, we have

$$\text{KL}(\pi_\gamma \parallel \mu_{t+1}^R) \leq (1 - \varepsilon) \text{KL}(\pi_\gamma \parallel \mu_t^R) + \varepsilon \text{KL}(\pi_\gamma \parallel \pi) \leq (1 - \varepsilon)^t \text{KL}(\pi_\gamma \parallel \mu_0^R) + \text{KL}(\pi_\gamma \parallel \pi)$$

and our upper bound is deduced from the Pinsker's inequality and Proposition 3,

$$\begin{aligned} \|\pi - \mu_t^R\|_{\text{TV}} &\leq \|\pi - \pi_\gamma\|_{\text{TV}} + \|\pi_\gamma - \mu_t^R\|_{\text{TV}} \\ &\leq (1 - \varepsilon)^{t/2} \sqrt{2 \text{KL}(\pi_\gamma \parallel \mu_0^R)} + 2 \sqrt{2 \text{KL}(\pi_\gamma \parallel \pi)}. \end{aligned}$$

A.4 Intermediate technical result

Before proving Theorem 2, we need an intermediate result.

Proposition 3. *Assume Conditions 3.1, 3.2, and 3.3 and $0 < \gamma \leq (2C_{\text{LS}}L^2)^{-1}$. Then R_γ has a unique stationary distribution π_γ that satisfies*

$$\text{KL}(\pi_\gamma \parallel \pi) \leq 4\gamma dL^2 C_{\text{LS}}.$$

Proof. As aforementioned, (6) implies that any compact set is small for R_γ and the Lebesgue measure is an irreducibility measure. Together with Condition 3.3 and Theorem 14.0.1 from Meyn and Tweedie [2012], this implies that for π_γ -almost-everywhere $x \in \mathbb{R}^d$,

$$\lim_{\ell \rightarrow \infty} \|R_\gamma^\ell(x, \cdot) - \pi_\gamma\|_{\text{TV}} = 0.$$

Furthermore, for all $x \in \mathbb{R}^d$ and $A \in \mathcal{B}(\mathbb{R}^d)$ such that $\text{Leb}(A) > 0$, we have $R_\gamma(x, A) > 0$; so $\pi_\gamma(A) = \pi_\gamma R_\gamma(A) > 0$ and so $\pi_\gamma \gg \text{Leb}$. Finally, for any $\nu \in \mathbb{M}_1$

$$\|\nu R_\gamma^\ell - \pi_\gamma\|_{\text{TV}} \leq \int \nu(dx) \|R_\gamma^\ell(x, \cdot) - \pi_\gamma\|_{\text{TV}},$$

and by the Lebesgue dominated convergence theorem it follows that

$$\lim_{\ell \rightarrow \infty} \|\nu R_\gamma^\ell - \pi_\gamma\|_{\text{TV}} = 0. \quad (11)$$

In Vempala and Wibisono [2019] (Theorem 1), it is shown that for all $\ell > 0$

$$\text{KL}(\nu R_\gamma^\ell \parallel \pi) \leq \exp(-C_{\text{LS}}\gamma\ell/2) \text{KL}(\nu \parallel \pi) + 4\gamma dL^2 C_{\text{LS}}.$$

Thus, the lower semi-continuity of the Kullback-Leibler for the weak topology [Van Erven and Harremos, 2014, Theorem 19] and the convergence in total variation distance of (11) imply that

$$\text{KL}(\pi_\gamma \parallel \pi) \leq \liminf_{\ell \rightarrow \infty} \text{KL}(\nu R_\gamma^\ell \parallel \pi) \leq 4\gamma dL^2 C_{\text{LS}}$$

where ν is such that $\text{KL}(\nu \parallel \pi) < \infty$. □

B Additional elements on the Gaussian mixture benchmarks

This section presents additional experimental details and results for the Gaussian mixture benchmarks introduced in Section 4.1, including ambient dimensions not shown in the main paper.

B.1 Additional sliced Wasserstein distances

Figure 6 illustrates the evolution of the sliced Wasserstein distance $\text{SW}_2(\mu_t, \pi)$ across EM2C iterations t for the corresponding settings. Across all configurations, the observed trends are consistent with those discussed in the main paper: smaller values of the mixing parameter λ lead to improved approximation of the target distribution.

Table 3 reports final sliced Wasserstein distances $\text{SW}_2(\mu_T, \pi)$ for the various target distributions. These results complement the GM4 experiments presented in Section 4 and provide a broader quantitative assessment of EM2C across different target distributions, dimensions, and exploration kernels.

B.2 Additional qualitative evolution plots

We report additional qualitative visualizations of EM2C proposal evolution (Figures 8, 9, and 7) analogous to Figure 3. They illustrate the effect of the mixing parameter λ and the exploration kernel on the ability of EM2C to recover and maintain multimodal structure.

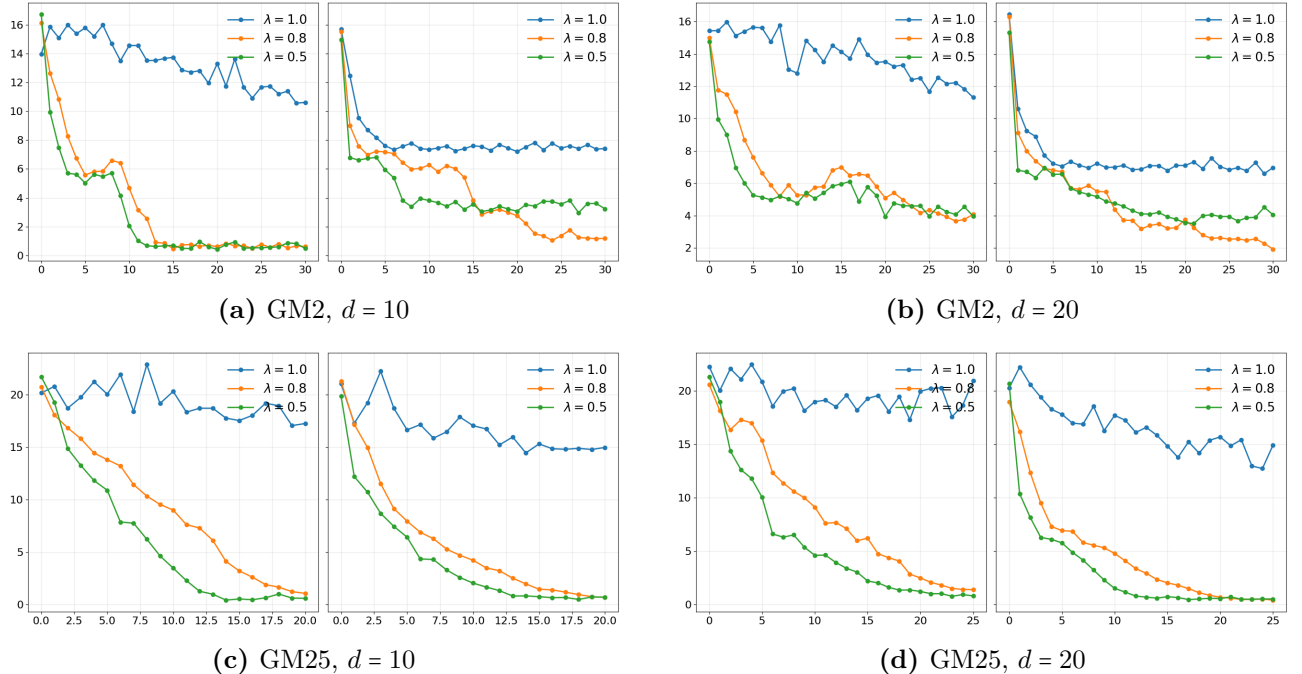


Figure 6: Evolution of the sliced Wasserstein distance $\text{SW}_2(\mu_t, \pi)$ over EM2C iterations for additional Gaussian mixture benchmarks. Results are shown for Random Walk (RW, left) and Unadjusted Langevin Algorithm (ULA, right) kernels and for mixing parameters $\lambda \in \{0.5, 0.8, 1.0\}$.

B.3 Comparison with Markov chain Monte Carlo

We provide a qualitative comparison between EM2C and a standard Markov MCMC sampler on the GM4 target distribution with dimension $d = 10$. The MCMC baseline is the Unadjusted Langevin Algorithm (ULA), which was observed to yield the best performance among the exploration kernels considered within EM2C.

To ensure a fair comparison, we match the overall computational budget between the two approaches. In EM2C, each iteration $t = 1, \dots, T$ applies the ULA exploration kernel for n_K steps to each particle. In the MCMC baseline, a single Markov chain is run for T outer iterations, and at each iteration the same ULA kernel is applied for n_K consecutive steps. As a result, the total number of MCMC transitions is equal to $n_K \times T$, matching the number of kernel applications used within EM2C.

Figure 10 illustrates the evolution of the ULA-based MCMC sampler under this matched computational budget. In contrast to EM2C, which maintains a population of particles, the single-chain MCMC sampler exhibits slower mode exploration and delayed coverage of the target distribution under the same budget.

B.4 Variational projection onto tensorized mixtures

Variational family. Throughout all experiments, the proposal distribution μ_t is chosen from a family of *tensorized Gaussian mixture models*. The ambient space \mathbb{R}^d is decomposed into $d/2$ disjoint two-dimensional blocks, and the proposal density is defined as a product of block-wise mixtures:

$$\mu_\theta(x) = \prod_{j=1}^{d/2} \mu_\theta^{(j)}(x^{(j)}), \quad x^{(j)} \in \mathbb{R}^2.$$

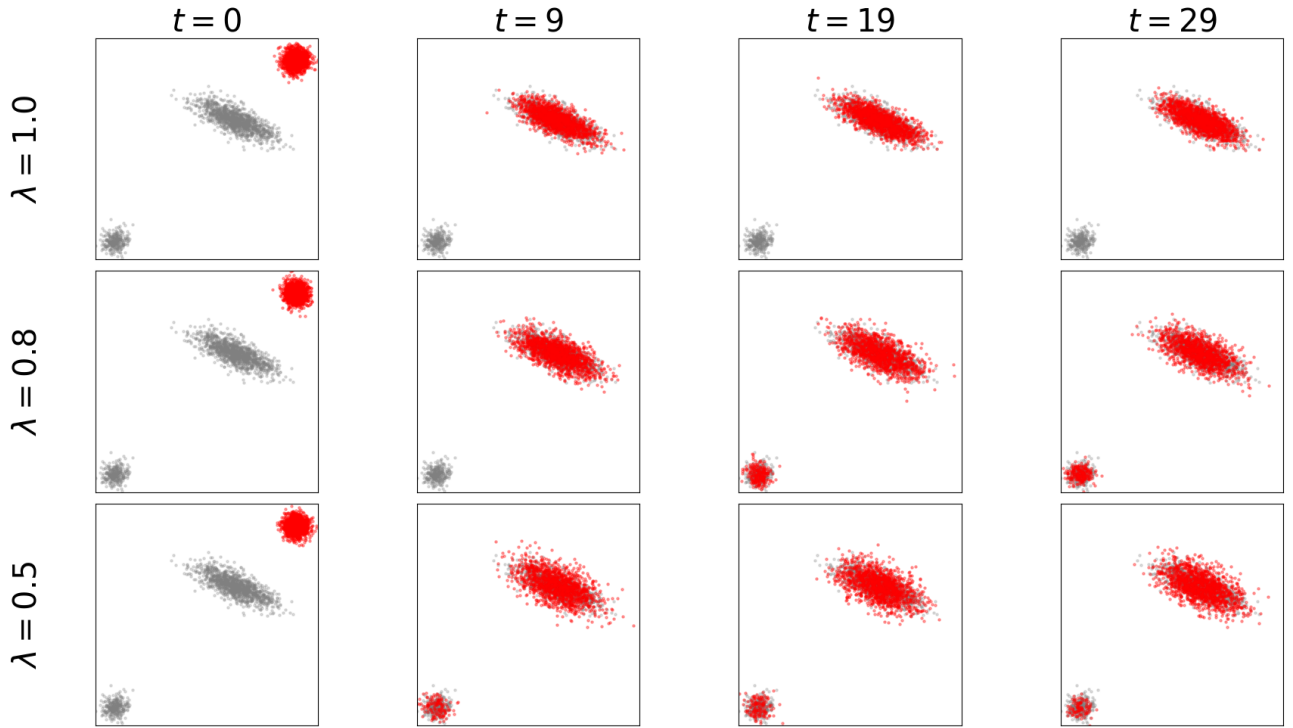
Each block marginal $\mu_\theta^{(j)}$ is a two-dimensional Gaussian mixture with K_0 components,

$$\mu_\theta^{(j)}(x^{(j)}) = \sum_{k=1}^{K_0} w_k^{(j)} \mathcal{N}\left(x^{(j)} \mid m_k^{(j)}, \Sigma_k^{(j)}\right),$$

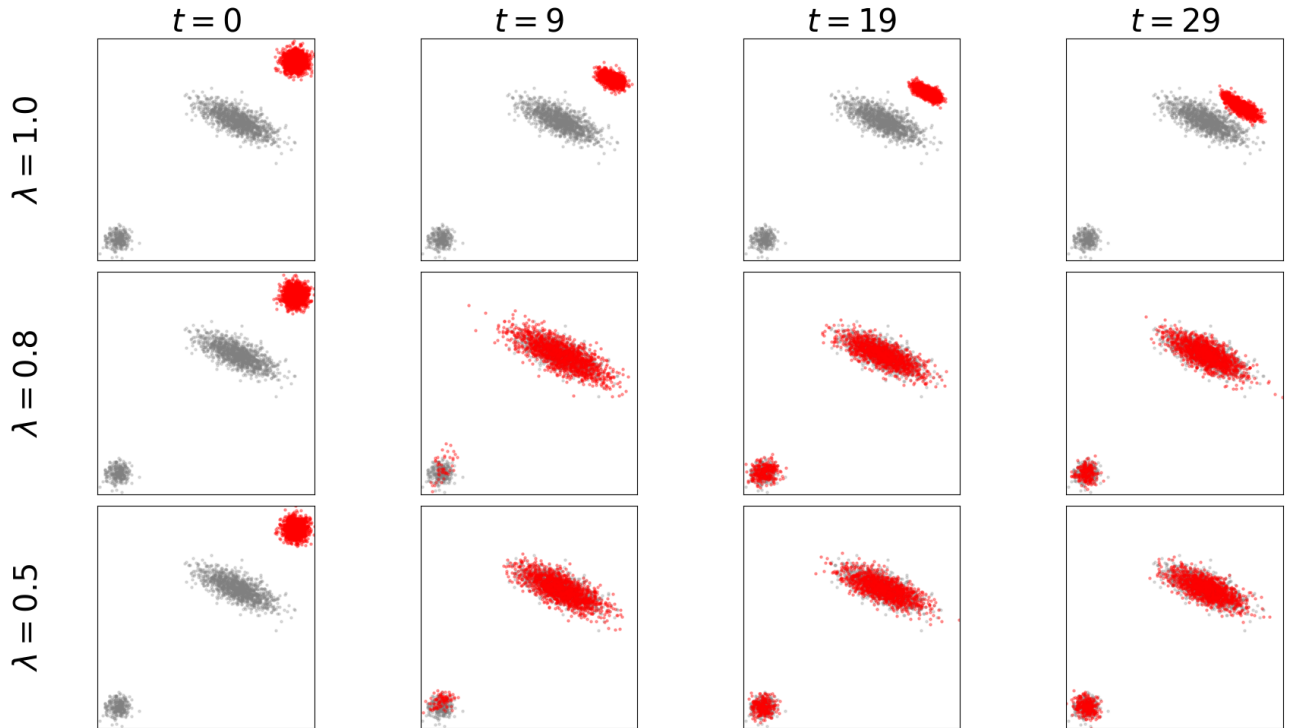
where the weights $w_k^{(j)}$ sum to one and the covariance matrices $\Sigma_k^{(j)}$ are full. The number of components K_0 is chosen to match the local multimodality of the target two-dimensional

Table 3: Final sliced Wasserstein distances for Gaussian mixture benchmarks GM2, GM4, and GM25 at various ambient dimensions, using either a Random Walk (RW) or Unadjusted Langevin Algorithm (ULA) kernel.

(a) GM2				(b) GM4				(c) GM25			
d	λ	RW	ULA	d	λ	RW	ULA	d	λ	RW	ULA
4	1.0	8.66	7.00	10	1.0	20.87	20.94	10	1.0	18.78	14.82
	0.8	7.37	2.31		0.8	7.10	0.63		0.8	2.63	0.60
	0.5	4.84	4.30		0.5	0.79	0.90		0.5	0.88	0.36
10	1.0	10.62	7.41	20	1.0	23.42	24.03	20	1.0	17.25	14.97
	0.8	0.62	1.19		0.8	6.35	5.74		0.8	1.08	0.70
	0.5	0.49	3.23		0.5	1.64	3.95		0.5	0.61	0.72
20	1.0	11.81	7.39						1.0	20.96	14.94
	0.8	3.83	1.59						0.8	1.39	0.42
	0.5	3.19	4.01						0.5	0.81	0.52



(a) Unadjusted Langevin Algorithm (ULA).



(b) Random Walk Metropolis (RW).

Figure 7: Evolution of EM2C proposals for the GM2 target in dimension $d = 10$. Rows correspond to $\lambda \in \{0.5, 0.8, 1.0\}$ and columns to successive EM2C iterations. For visualization purposes, only the two-dimensional projection onto coordinates (x_0, x_1) is displayed. Gray points denote samples from the target distribution π , and red points the learned proposal μ_t .

marginals: $K_0 = 2$ for GM2, $K_0 = 4$ for GM4, and $K_0 = 25$ for GM25. This tensorized construction implicitly defines a mixture with $K_0^{d/2}$ components in dimension d .

Projection via expectation–maximization. At each EM2C iteration, the ideal update is approximated by an empirical measure $\widehat{\mu}_{t+1}$ represented by a set of particles $Z_t^{1:N}$. The projection onto the variational family is performed independently for each two-dimensional block. For block j , we extract the projected samples

$$Z_{t,j}^{(i)} \in \mathbb{R}^2, \quad i = 1, \dots, N,$$

and estimate the parameters of the corresponding Gaussian mixture $\mu_\theta^{(j)}$ by maximum likelihood using the EM algorithm.

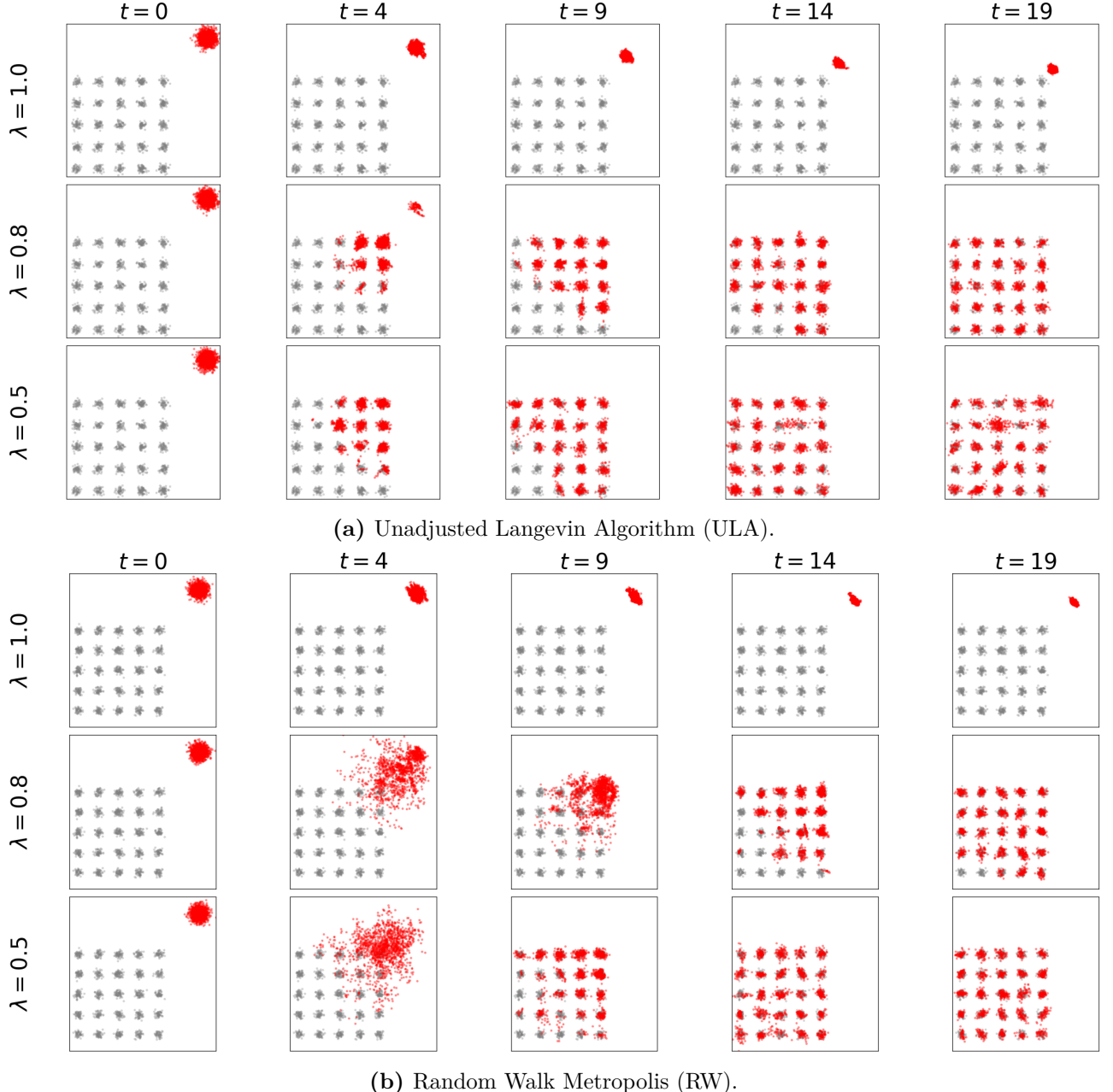
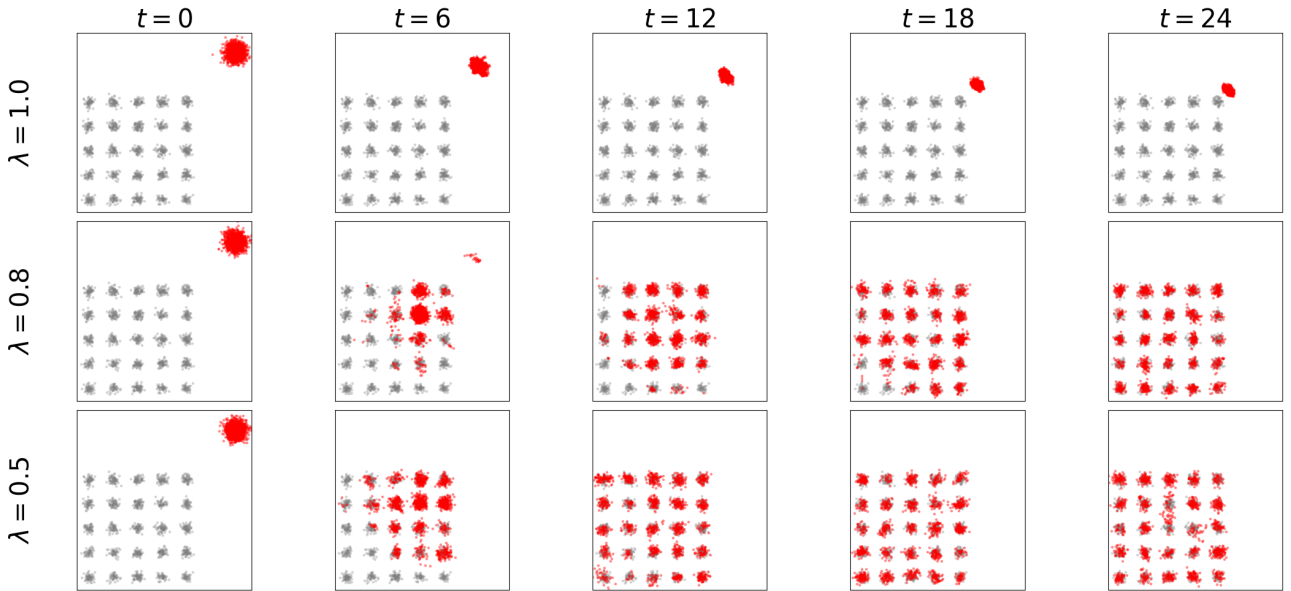
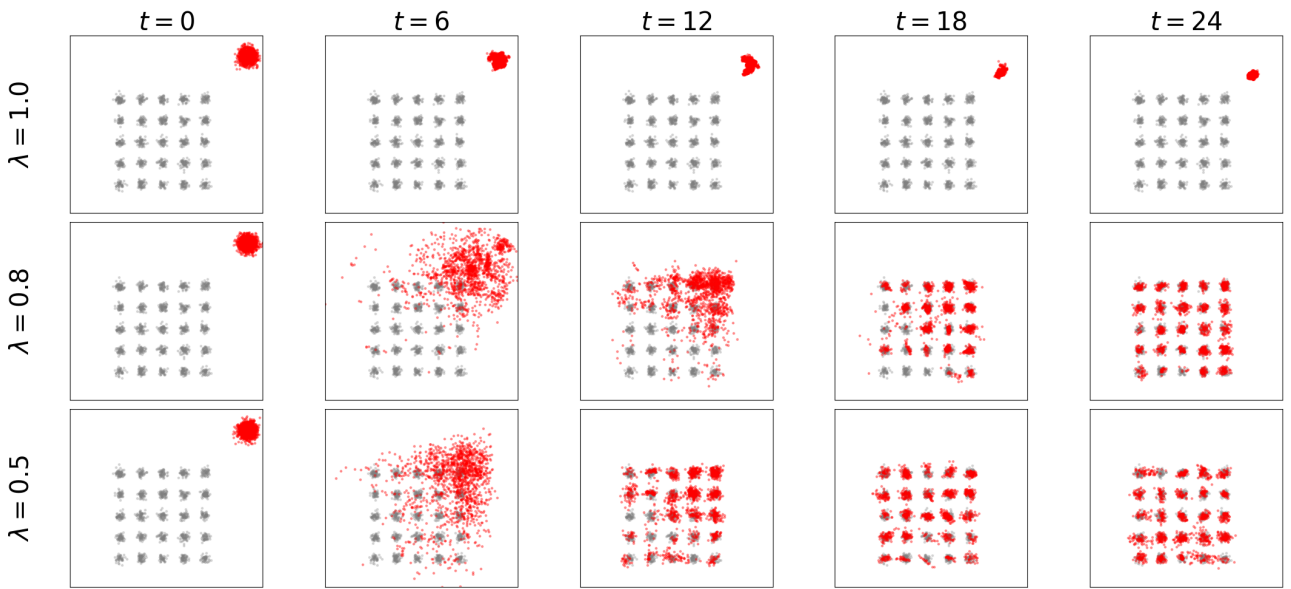


Figure 8: Evolution of EM2C proposals for the GM25 target in dimension $d = 10$. Rows correspond to $\lambda \in \{0.5, 0.8, 1.0\}$ and columns to successive EM2C iterations. For visualization purposes, only the two-dimensional projection onto coordinates (x_0, x_1) is displayed. Gray points denote samples from the target distribution π , and red points the learned proposal μ_t .



(a) Unadjusted Langevin Algorithm (ULA).



(b) Random Walk Metropolis (RW).

Figure 9: Evolution of EM2C proposals for the GM25 target in dimension $d = 20$. Rows correspond to $\lambda \in \{0.5, 0.8, 1.0\}$ and columns to successive EM2C iterations. For visualization purposes, only the two-dimensional projection onto coordinates (x_0, x_1) is displayed. Gray points denote samples from the target distribution π , and red points the learned proposal μ_t .

EM hyperparameters. Each two-dimensional Gaussian mixture is fitted using the standard EM algorithm with full covariance matrices, k-means++ initialization, $n_{\text{init}} = 3$ random restarts, a maximum of 500 iterations, and a covariance regularization parameter of 10^{-3} . All EM fits are performed independently across blocks and EM2C iterations.

B.5 Experimental configurations

We provide here a complete description of the experimental configurations used for the GM2, GM4 and GM25 benchmarks. Namely, we report in Table 4, the kernel hyperparameters (RW: step size σ_K , ULA: step size γ_K), the number of kernel steps n_K applied at each EM2C iteration, and the total number of EM2C iterations T . These configurations are adapted to the

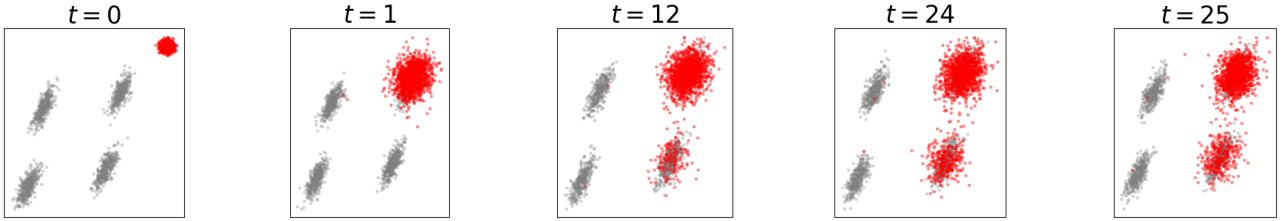


Figure 10: Evolution of a standard Markov chain Monte Carlo (MCMC) sampler based on the Unadjusted Langevin Algorithm (ULA) for the GM4 target distribution in dimension $d = 10$. Snapshots are shown at successive outer iterations t , where each iteration corresponds to n_K consecutive applications of the ULA transition kernel. The total number of MCMC transitions is therefore equal to $n_K \times T$, matching the computational budget used by EM2C. Gray points denote samples from the target distribution π , and red points correspond to the current state of the Markov chain.

Table 4: Exploration kernel parameters (RW: σ_K , ULA: γ_K), numbers of kernel steps n_K , and numbers of EM2C iterations T used for the Gaussian mixture benchmarks.

(a) GM2					(b) GM4					(c) GM25				
d	Kernel	σ_K/γ_K	n_K	Td	Kernel	σ_K/γ_K	n_K	T	Kernel	σ_K/γ_K	n_K	T		
2, 4	RW	6.0	20	2, 4, 10	RW	4.5	15	254	RW	1.5	10	15		
10	RW	8.0	20	3, 20	RW	5.0	15	25	RW	2.0	15	20		
20	RW	7.0	20	3, 2, 4, 10, 20	ULA	2.0	10	25	RW	2.5	20	25		
2, 4	ULA	2.3	15	25				2, 4	ULA	0.3	10	15		
10, 20	ULA	2.3	15	30				10	ULA	0.3	10	20		
								20	ULA	0.35	10	25		

scale and geometry of each target distribution and were selected to ensure stable exploration across dimensions.

C Additional elements on the two-dimensional benchmarks of Section 4.2

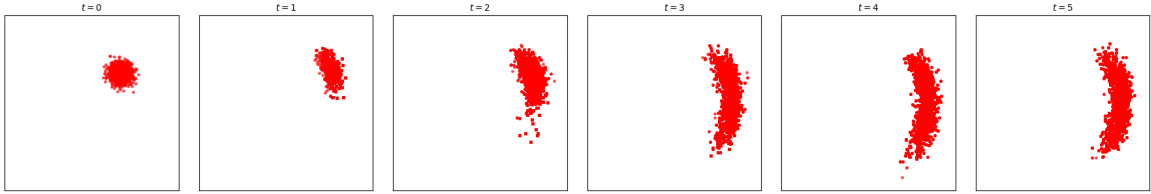
This section presents additional experimental details and results for the the two-dimensional benchmarks introduced in Section 4.2

C.1 Additional qualitative evolution plots

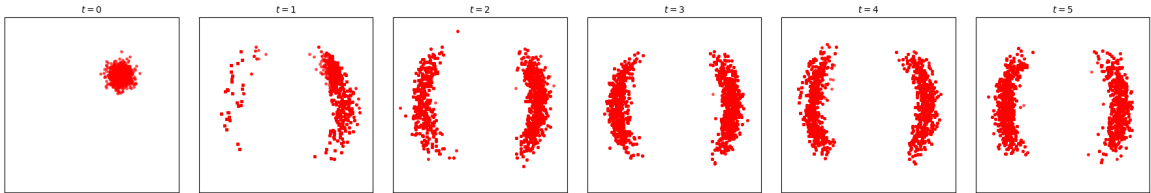
Figures 11 and 12 show the evolution of a reweighted samples from the EM2C proposal distributions for the Dual Moons and Two Rings benchmarks, respectively, for mixing parameter $\lambda = 1.0$ and $\lambda = 0.8$. Each panel displays samples generated from the EM2C proposal distributions μ_t and subsequently resampled according to the importance $\pi(x)/\mu_t(x)$. This resampling step is performed solely for visualization purposes and removes samples with negligible contribution to the target distribution.

C.2 Variational projection using normalizing flows

The variational projection step in EM2C is implemented using a normalizing flow. This projection replaces the Gaussian mixture approximation used in the high-dimensional Gaussian

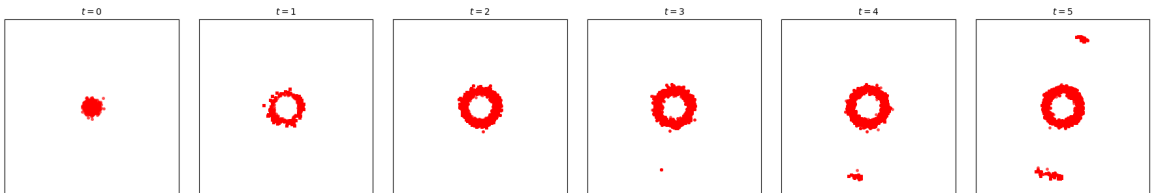


(a) $\lambda = 1.0$

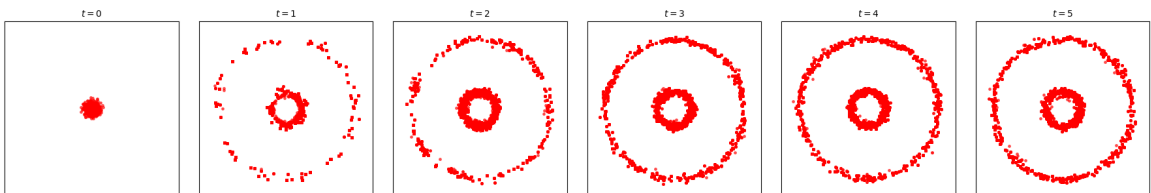


(b) $\lambda = 0.8$

Figure 11: Evolution of EM2C proposal distributions on the Dual Moons benchmark. Plotted samples are drawn from the intermediate proposals μ_t and resampled using importance weights $\pi(x)/\mu_t(x)$ for visualization.



(a) $\lambda = 1.0$



(b) $\lambda = 0.8$

Figure 12: Evolution of EM2C proposal distributions on the Two Rings benchmark. Plotted samples are drawn from the intermediate proposals μ_t and resampled using importance weights $\pi(x)/\mu_t(x)$ for visualization.

mixture benchmarks.

Flow configuration and training. Throughout all these experiments, the projection step is implemented using a Neural Spline Flow (NSF) with fixed architecture and training hyperparameters. The flow consists of three coupling transforms, each parameterized by a neural network with two hidden layers of width 64. Rational quadratic spline transformations with 8 bins are used in each coupling layer.

The flow is trained by maximum likelihood on $N = 10,000$ particles generated by EM2C, for 8 epochs, using a batch size of 256 and a learning rate of 10^{-3} . All flow hyperparameters are kept fixed across target distributions and experiments.

Table 5: Algorithm parameters for the Dual Moons and Two Rings benchmarks.

Method	Parameters	Dual Moons	Two Rings	Comments
MCMC (RW)	$\sigma_{\text{RW}}, n_{\text{iter}}$	1.0, 1,000	0.9, 1,000	Shared RW kernel
NUTS	$d_{\text{max}}, n_{\text{warmup}}$	3, 1,000	3, 1,000	Single chain, adaptive step size
AIS (RW)	$L, \sigma_{\text{RW}}, n_{\text{iter}}$	40, 1.0, 1,000	40, 0.9, 1,000	Same RW kernel as MCMC
EM2C	$\sigma_K, n_K, \sigma_L, n_L$	1.0, 10, 0.1, 5	0.9, 10, 0.1, 5	RW exploration and local move

C.3 Experimental configurations

We report here the initial distributions and the main hyperparameters associated with each algorithm used throughout experiments of Section 4.2.

Initial distributions For all methods, it is set to a Gaussian distribution $\mathcal{N}(m_0, \Sigma_0)$. For the Dual Moons distribution, we set $m_0 = (1.0, 1.0)^\top$ and $\Sigma_0 = 0.04I_2$. For the Two Rings distributions, we set $m_0 = (0.0, 0.0)^\top$ and $\Sigma_0 = 0.04I_2$.

Methods and hyperparameters To ensure a fair comparison across methods, all experiments are conducted using a fixed number of $N = 10,000$ particles. Moreover, whenever a Random Walk (RW) Markov kernel is employed, the same kernel configuration is used consistently across methods, namely in MCMC RW, Annealed Importance Sampling, and the exploration step of EM2C.

- **Markov chain Monte Carlo (MCMC).** We use a Random Walk (RW) Metropolis Hastings sampler with an isotropic Gaussian proposal with variance σ_{RW}^2 . The sampler is run as a single Markov chain for a fixed number of n_{iter} iterations and the final state is used for evaluation. We do not include the Unadjusted Langevin Algorithm (ULA) in these experiments, as gradient-based proposals were empirically less effective than RW in this low-dimensional and multimodal setting.
- **No-U-Turn Sampler (NUTS).** The step size is adapted automatically during a warmup phase of n_{warmup} iterations, with target acceptance probability fixed to 0.8. The maximum tree depth is set to d_{max} . After warmup, N samples are collected from the resulting chain.
- **Annealed Importance Sampling (AIS).** AIS is implemented using a linear annealing schedule $\{\beta_\ell\}_{\ell=0}^L$ interpolating between the initial proposal and the target distribution. At each intermediate temperature, particles are propagated using n_{iter} steps of a Random Walk (RW) Markov kernel invariant with respect to the corresponding intermediate distribution. As in the MCMC experiments, we use an isotropic Gaussian RW proposal. No resampling step is performed.
- **Entropic Mirror Monte Carlo (EM2C).** EM2C is run for $T = 6$ outer iterations with $\varepsilon = 0.8$ and $\lambda = 0.8$. At each iteration, exploration is performed using a Random Walk kernel applied for n_K steps with Gaussian variance σ_K^2 , followed by a local resample–move step using the same kernel with variance σ_L^2 for n_L steps. The projection step is implemented using a normalizing flow, as described in Appendix C.2.

The main hyperparameters used for the Dual Moons and Two Rings benchmarks are summarized in Table 5.

D Additional implementation details

This section summarizes implementation details used throughout the paper, including model-specific configurations, and the evaluation metrics used to assess performance.

D.1 Sliced Wasserstein distance

We quantify the discrepancy between the learned proposal distribution and the target distribution using the sliced Wasserstein distance. This metric is particularly well suited for high-dimensional distributions, as it avoids the curse of dimensionality associated with optimal transport in large dimensions while remaining sensitive to geometric discrepancies between probability measures.

Definition 1. Let μ and ν be two probability measures on \mathbb{R}^d with finite second moments. For a unit vector $\theta \in \mathbb{S}^{d-1}$, we denote by $\theta_{\#}\mu$ the pushforward of μ by the projection $x \mapsto \langle x, \theta \rangle$. The sliced Wasserstein-2 distance between μ and ν is defined as

$$\text{SW}_2(\mu, \nu) = \left(\int_{\mathbb{S}^{d-1}} W_2^2(\theta_{\#}\mu, \theta_{\#}\nu) \, d\theta \right)^{1/2}, \quad (12)$$

where W_2 denotes the one-dimensional Wasserstein-2 distance and the integral is taken with respect to the uniform distribution on the unit sphere \mathbb{S}^{d-1} .

Empirical computation. In practice, the integral in (12) is approximated by Monte Carlo. Given samples $\{x_i\}_{i=1}^N \sim \mu$ and $\{y_i\}_{i=1}^N \sim \nu$, we draw independent random directions $\{\theta_k\}_{k=1}^K$ uniformly on \mathbb{S}^{d-1} . For each direction θ_k , we compute the one-dimensional projections $\langle x_i, \theta_k \rangle$ and $\langle y_i, \theta_k \rangle$, sort them, and evaluate the squared Wasserstein-2 distance in closed form. The resulting estimator reads

$$\widehat{\text{SW}}_2(\mu, \nu) = \left(\frac{1}{K} \sum_{k=1}^K \frac{1}{N} \sum_{i=1}^N \left(x_{(i)}^{(k)} - y_{(i)}^{(k)} \right)^2 \right)^{1/2},$$

where $x_{(i)}^{(k)}$ and $y_{(i)}^{(k)}$ denote the sorted projected samples along direction θ_k .

Implementation details. We computed the sliced Wasserstein distance using $N = 2,000$ samples drawn from both the proposal distribution μ_t and the target distribution π on the Gaussian mixture benchmarks, and $N = 10,000$ for the two-dimensional benchmarks of Section 4.2.

The integral over the unit sphere in (12) is approximated using $K = 100$ random projection directions sampled uniformly from \mathbb{S}^{d-1} . For a given experiment, the same set of target samples is reused across all EM2C iterations t , while proposal samples are resampled at each iteration.

D.2 Energy distance

In addition to the sliced Wasserstein distance, we also report the energy distance for the two-dimensional benchmarks of Section 4.2. The energy distance is a discrepancy measure defined for probability measures on \mathbb{R}^d . It provides a complementary notion of discrepancy between the learned proposal distribution and the target distribution that is sensitive to differences in both location and spread.

Definition 2. Let $X \sim \mu$ and $Y \sim \nu$ be random variables in \mathbb{R}^d , and let X' and Y' denote independent copies of X and Y , respectively. The energy distance between μ and ν is defined as

$$\text{ED}(\mu, \nu) = 2\mathbb{E}[\|X - Y\|] - \mathbb{E}[\|X - X'\|] - \mathbb{E}[\|Y - Y'\|].$$

Empirical computation. Given samples $\{x_i\}_{i=1}^N \sim \mu$ and $\{y_j\}_{j=1}^N \sim \nu$, we estimate the energy distance using the empirical estimator

$$\widehat{\text{ED}}(\mu, \nu) = 2 \frac{1}{N^2} \sum_{i,j} \|x_i - y_j\| - \frac{1}{N^2} \sum_{i,i'} \|x_i - x_{i'}\| - \frac{1}{N^2} \sum_{j,j'} \|y_j - y_{j'}\| .$$

Implementation details. The energy distance is computed using $N = 10,000$ samples drawn from both the proposal distribution μ_t and target distribution π .

D.3 Optional local move kernel

In Algorithm 1, the particles $Z_t^{1:N}$ are obtained by resampling from the empirical mixture $\widehat{\mathcal{F}}_{\tilde{\mu}_t}^N$ defined at iteration t , which may result in reduced diversity among the resampled particles. In the numerical experiments, we optionally apply an additional local Markov transition to these particles prior to the variational projection step. More precisely, after sampling

$$Z_t^i \sim \widehat{\mathcal{F}}_{\tilde{\mu}_t}^N, \quad i = 1, \dots, N ,$$

as described in Algorithm 1, we apply a local Markov kernel L independently to each particle, yielding

$$\tilde{Z}_t^i \sim L(Z_t^i, \cdot), \quad i = 1, \dots, N .$$

The minimization of the loss within Algorithm 1 is then performed using the transformed particles $\tilde{Z}_t^{1:N}$ in place of $Z_t^{1:N}$.

The sole purpose of the local kernel L is to mildly disperse highly concentrated particle clouds that may arise after resampling, thereby improving numerical stability in early iterations. For this reason, the local move kernel is omitted from Algorithm 1 in the main text for clarity. All experimental results reported in the paper are consistent with the simplified formulation of Algorithm 1, and the optional local move kernel only affects the numerical behaviour of the Monte Carlo implementation.